Строительные материалы и изделия
Construction Materials and Products

journal homepage: https://bstu-journals.ru

ISSN
2618-7183

DOI: 10.58224/2618-7183-2025-8-3-9

Evaluation of timber-fiber reinforced polymer composite systems: experimental study and reliability analysis

Larah R. Abdulwahed * [1]

[1] Baquba Technical College, Middle Technical University, Diyala, Iraq

Abstract. Timber, an ancient material widely used in construction, possesses unique properties but exhibits relative brittleness, particularly in bending. To enhance the performance and reinforce wooden structures, the incorporation of fiber-reinforced polymer (FRP) components has been proposed as a viable solution. However, the timber-FRP system has received less attention compared to the concrete-FRP system in literature, resulting in limited prediction models. Thus, the reliability of these models requires further examination. This research presents an experimental investigation aimed at evaluating the bond strength of timber members strengthened by FRPs, utilizing a pull-out test with various FRP sheets and adhesives. The acquired data is combined with existing experimental data from the literature to propose a novel probabilistic regression model. Furthermore, a comprehensive reliability analysis of the timber-FRP system is conducted by gathering models previously presented by researchers. These models are then compared with the newly developed probabilistic models. Considering three loading levels and defining uncertainty in six influential variables, 192 first-order reliability analyses are performed in two scenarios: one incorporating the model factor and the other without it. The results reveal a significant decrease in the reliability index when uncertainties are considered during member design. The existing models exhibit an average reliability index decrease from 4.26 to 2.82. Additionally, as anticipated, the influence of the live/dead load ratio on determining the reliability index diminishes in the presence of uncertainties.

Keywords: Timber, Fiber Reinforced Polymer (FRP), Bond Strength, Reliability Analysis, Probabilistic Regression Model, Structural Strengthening

Please cite this article as: Larah R. Abdulwahed evaluation of timber-fiber reinforced polymer composite systems: experimental study and reliability analysis. Construction Materials and Products. 2025. 8 (3). 9. DOI: 10.58224/2618-7183-2025-8-3-9

*Corresponding author E-mail: dr.larah.riyadh@mtu.edu.iq

Received February 1, 2025; Received in revised form April 4, 2025; Accepted June 6, 2025

1. INTRODUCTION

Fiber reinforced polymer (FRP) components, characterized by high-strength fibers embedded in a polymeric matrix, have gained significant attention due to their lightweight nature, ease of implementation, and unique properties such as high tensile strength, corrosion resistance, and fatigue resistance [1]. Consequently, engineers have increasingly utilized FRP in various types of structures, including concrete, masonry, and timber structures. The most commonly employed types of FRP in these applications are carbon (CFRP), glass (GFRP), and aramid (AFRP). The primary objective of incorporating FRP is to enhance the strength and ductility of structural elements such as bridges, dams, pipelines, and other components. Numerous FRP reinforcement systems have been developed for masonry and concrete structures, as evidenced in the literature [2-6].

While timber is a renewable and recyclable construction material with widespread application, certain inherent flaws require thorough investigation. These flaws include biological deterioration over time and brittle behavior in flexural loading. Strengthening timber members with FRP and adhesive represents a promising technique to mitigate these shortcomings and enhance the strength and stiffness of timber structures. Previous studies have explored aspects such as the adhesion quality of timber-FRP using various types of adhesives and FRP plates [7-10]. The thermal stability of the timber-FRP system employing epoxy [11, 12], and the reinforcement of wooden beams through FRP sheets and a prestressing system [13, 14]. Additionally, alternative materials such as nanoclay, glass, and carbon fibers have been investigated to improve wood properties [5, 15].

Wood and FRP possess a fibrous structure that lends itself well to bonding with an adhesive matrix. Unlike wood, FRP sheets do not experience a natural reduction in resistance over time. The evaluation of timber-FRP bond quality typically involves two distinct setups. Modified versions of ISO 6238 (2001) and ASTM D905-03 (2003) tests have been employed by various researchers to assess the shear strength of the bond between the FRP plate and the timber surface, providing a mean stress value. However, these tests do not investigate the strain behavior of the FRP plates within the timber interface. To address this limitation, other researchers have utilized single-shear and double-shear bonding methods in the timber-FRP system, facilitating the monitoring of the FRP interface and enabling the development of interface models [16-18].

The configuration of single and double shear tests represents the second failure mode of the bonded interface and provides valuable experimental data, including bond strength, strain distribution, shear stress distribution, and slip stress response. These results are crucial for numerical simulations of the bonding interface and its failure [19, 20]. Extensive experiments have been conducted on the strength and bonding behavior of FRP with concrete, with single shear testing being the prevalent configuration [21, 22]. Researchers have also explored the strength and bonding behavior of FRP with steel using single and double shear tests, although there have been fewer studies on steel-FRP compared to concrete-FRP.

In concrete-FRP connections, debonding failure often occurs in the concrete layer due to the adhesive typically being stronger than concrete. In steel-FRP connections, failure can occur in the adhesive, the steel and adhesive interface, and the FRP and adhesive interface [23,24]. However, experiments investigating FRP bonding to wood using single and double shear tests are limited, leading to ongoing development of stress-slip models. Researchers investigated the behavior of FRP externally bonded to timber. A novel theoretical model was developed to predict composite behavior by 136 single shear FRP-to-timber joints as well as explored the behavior of bond mechanisms in FRP composites externally bonded to timber [25, 26]. The study noted that the bond strength significantly increased with increase in bond width and timber tensile strength. It also contained a numerical simulation where a finite element analysis could effectively predict the composite behavior by choosing appropriate constitutive models for materials.

Repairs involving the use of Fiber Reinforced Polymers (FRP) employ various connection systems. One commonly utilized method is the wet layup technique, which entails the placement of dry fibrous sheets or resin-impregnated fabrics in situ. This approach, introduces involves the adhesion of FRP plates to the material's surface using a resin and primer layer, followed by on-site curing. Initially, studies primarily focused on bonding FRP sheets to concrete elements [27-29]. Kaiser and Karbhari

were the first to investigate the impact of uncertainties in composites produced through the wet layup method [30, 31]. They identified potential defects in the system, such as fiber rupture, inappropriate resin mixtures with impurities, in-situ fabrication errors, and the penetration of moisture or chemicals. Despite the inherent uncertainties associated with this method, which lead to a wide range of variation in results, the wet layup technique is frequently employed in repairs due to its flexibility for on-site applications and cost-effectiveness compared to other methods [32, 33].

In the realm of construction materials, the application of machine learning and regression techniques has revolutionized the way engineers analyze and predict material properties [34-36]. By harnessing vast amounts of data on material composition, performance under different conditions, and environmental factors, machine learning algorithms can uncover complex patterns that traditional methods might overlook. Regression models, in particular, play a crucial role in predicting material behaviors based on various input parameters [35, 37, 38]. Through these advanced techniques, engineers can optimize material selection, anticipate potential weaknesses, and ensure structural integrity. Moreover, by integrating reliability analysis into these predictive models, stakeholders can gain deeper insights into the probability of material failure under different scenarios, thus enhancing the robustness and safety of construction projects.

Reliability analysis has found applications in various fields of civil engineering, including FRP composites. Atadero and Karbhari conducted a reliability-based design study to calibrate resistance factors for externally-bonded FRP composites [39, 40]. They investigated the flexural rehabilitation of reinforced concrete T-beam bridge girders using carbon fiber-reinforced composites as a case study. Zhou and coworker performed a reliability-based design analysis on reinforced concrete beams, considering different FRP configurations such as U-jacketing, side bonding, and complete wrapping [41, 42]. They assessed the accuracy of existing models from the literature and identified the most suitable model for each configuration. A reliability-based approach to investigate the seismic performance of reinforced concrete frames with FRP laminates was applied considering environmental conditions and specific loadings [43]. Reliability analysis of FRP composites subjected to wet-dry cycles was conducted, focusing on the degradation of FRP laminates under harsh environmental conditions [44]. They calculated reliability indices and demonstrated that wet-dry cycles adversely affected tensile strength while minimally impacting the elastic modulus. Chang and his team examined the effect of uncertainties in existing structures and FRP on structural repairs [45, 46]. They identified that the most critical uncertainties in structural restoration are related to the area of steel reinforcement and the strength of the existing structure. Zhang and workers, considering the uncertainties in their model, investigated the probabilistic analysis of the concrete-FRP bond [47]. They proposed valuable recommendations for structural strengthening, incorporating eight models from literature.

Existing models on the pullout strength of timber-FRP composites have employed various tools to propose predictive models. Benedetti and colla calculated ultimate anchorage force with fracture mechanics concepts using experimental datasets [48]. Also, Juvandes and Barbosa implemented a bond analysis of timber structures strengthened with FRP systems [49]. They calibrated a previously-proposed model to predict the maximum anchor strength of the composite. They also recommended some design criteria. The authors used softwood in the timber-FRP composite and proposed a predictive model with different variables [8, 50]. A new model to predict the stress and strain distribution profiles along the interface of timber and FRP was developed [25, 51]. Palizi and Toufigh used machine learning approach to propose a predictive model based on gene expression programming. They also proposed other models to predict the bond stress reduction of timber-FRP composites in acidic/alkaline conditions [37]. Based on the literature investigations, limited research existed considering uncertainties of the variables in a model. While reliability analysis of FRP composites has predominantly focused on concrete elements, there is a noticeable absence of probabilistic studies pertaining to the timber-FRP system. Thus, there is a pressing need to initiate studies in this direction.

This paper aims to examine the impact of uncertainties on the reliability of timber-FRP composites. To accomplish this, a novel Bayesian model is introduced, incorporating data obtained from literature sources and an experimental program. The effectiveness of the model will be evaluated, followed by an investigation into the uncertainty effects on the reliability of existing deterministic models from previous studies. Overall, the results of this study highlight the pressing need for robust prediction

models within the timber-FRP system domain, especially considering their relatively limited exploration compared to concrete-FRP systems. The proposed Bayesian model, which integrates both empirical and literature-derived data, offers a promising approach to enhancing the reliability of predictive tools in this field. Moreover, the identification of a significant decrease in reliability indices when uncertainties are incorporated into member design underscores the importance of accounting for uncertainties in structural assessments, thereby providing valuable insights for both practitioners and researchers.

2. METHODS AND MATERIALS

It is demonstrated that the enhancement of mechanical properties in the timber-FRP system is significant, and the bond strength quality is more than the same composite with concrete or steel [13]. Accordingly, the efficiency of this system for retrofitting is not hidden from anyone. Nevertheless, one of the most common failures in this system is debonding of FRP composite adhesive where the total capacity of FRP is not consumed, and the desired ductility of the structural system is not provided. Hence, it is concluded that the adhesive's performance directly affects the composite's performance. Various models based on empirical relationships or failure theories have been proposed in this regard. However, a lack of efficient models still exists in the wood-FRP system compared to the concrete-FRP system. Table 1 illustrates the proposed models for the wood-FRP system.

Table 1. Proposed models for bond strength timber-FRP system.

Model Number	Model Name	Model
1	[48]	$P_u = \frac{1}{2} b_f f_{ts} \sqrt{\frac{E_f t_f}{2 f_{ts}}}$
2	[49]	$P_u = P_{max} \frac{L_b}{L_e} (2 - \frac{L_b}{L_e})$ $P_{max} = c_1 k_b k_c K_\mu b_f \sqrt{E_f t_f \tau_{max}}$ $L_e = \sqrt{\frac{E_f t_f}{c_2 \tau_{max}}}$ $k_b = 1.06 \sqrt{\frac{2 - \frac{b_f}{b_w}}{1 + \frac{b_f}{400}}} \quad 1 \le k_b \le 1.29$
3	[52]	$P_u = 0.012 \gamma_w \gamma_a b_f L_e^{0.28} \sqrt{E_f t_f}$ $\tau(x) = \frac{\partial J}{\partial \delta} = A^2 B C_N e^{-Bs} (1 - e^{-Bs})$ $J = \frac{1}{2} C_N P^2$ $C_N = \left(\frac{1}{b_f}\right)\left(\frac{1}{C_w} + \frac{1}{C_f} + \frac{(t_w + t_f + 2t_a)^2}{4 D_w}\right)$ $P = A(1 - e^{-Bs})$

Continuation of Table 1

4	[53]	$P_u = \gamma_w \sqrt{L_e f_{ts} E_f t_f \left(\frac{b_f}{b_w}\right)^3}$ $\tau(x) = \frac{6P}{b_f L_e^2}\left(1 - \frac{x}{L_e}\right)x$ $\tau(max) = \frac{3P_u}{2b_f L_e}$ $L_e = \alpha\beta(f_{ts})^{0.25}\ln(E_f t_f)$ $\beta = \frac{1.25 + \frac{b_f}{b_w}}{2\left(2.5 - \frac{b_f}{b_w}\right)}$
5	[35]	$\frac{F}{E_t A_t} = \left\{ \begin{array}{l} \left(\left(\frac{E_{ad}}{E_f}\right)^6 (C4.C0.C1) \frac{S_{ad}}{S_f} \left(\left(\frac{S_{ad}}{S_f} - C2\right)^3 - \sqrt{C3\frac{E_{ad}}{E_f}} \right) \right)^3 \\ + \left(\left(\left(C7 + \frac{A_{ad}}{A_f} + \frac{E_{ad}}{E_f}\frac{A_{ad}}{A_f} \right) \sqrt{\frac{E_{ad}}{E_f}} \right) + \left(\left(\frac{S_{ad}}{S_f} - C8\right) C5.C8 \right) \right) \left(C6^3 + \left(\frac{S_{ad}}{S_f}\right)^2 \right)^3 \end{array} \right\}$

where P_u is the maximum applied load, b_f, t_f, and E_f are the width, thickness, and elasticity modulus of FRP sheets. b_w, t_w, and E_w are the width, thickness, and elasticity modulus of timber, respectively. f_{ts} is the tensile strength, G_a and t_a are shear modulus of adhesive, and L_b and L_e are bond length and effective length of bond. τ and $\tau(max)$ represent the bond strength and the maximum shear stress of the bond. *A*, *B*, *a*, and *C1-C8* are constants according to the main studies. c_1 and c_2 are empirically equal to 0.7 and 10. The factor k_c is a symbol of surface preparation and relies between 0.67 to 1.0. The k_μ factor is the strengthening level that can be assumed as 1.0. γ_w and γ_a determine the direction of the wood and the adhesive. C_N, C_w, and C_f are elastic stiffness, wood axial stiffness, and FRP axial stiffness, respectively.

In this study, a comprehensive approach was adopted, comprising both experimental investigations and literature review. The experimental phase involved the implementation of a series of tests aimed at adding them to the collected data from previous studies, forming a robust dataset. Subsequently, this combined dataset served as the foundation for the development of a novel predictive model. Concurrently, various pre-existing models documented in the literature were meticulously collected for the purpose of conducting a thorough reliability analysis. Through this analysis, the performance and efficacy of these existing models were critically evaluated. The outcomes of the reliability analysis were then compared to the newly developed probabilistic model, enabling a comprehensive comparison of their predictive capabilities. This comparative analysis served as a means to ascertain the effectiveness and superiority of the proposed model over existing alternatives, thereby contributing to the advancement of predictive modeling methodologies.

3. RESULTS AND DISCUSSION

3.1. Test details

Table 2 summarizes the experimental program in this research. According to this table, one type of wood, three types of FRP with two different thicknesses, and three types of adhesive were considered for preparing the timber-FRP specimens for the pull-out test. Overall, three specimens were prepared for each experiment, resulting in 54 specimens.

Table 2. The experimental program.

Sample No.	Timber	FRP	FRP thickness (mm)	Adhesive	Number of tested samples
1	Hardwood	Carbon	0.16	30	3
2		Aramid	0.16	30	
3		Glass	0.16	30	
4		Carbon	0.32	30	
5		Aramid	0.32	30	
6		Glass	0.32	30	
7		Carbon	0.16	300	
8		Aramid	0.16	300	
9		Glass	0.16	300	
10		Carbon	0.32	300	
11		Aramid	0.32	300	
12		Glass	0.32	300	
13		Carbon	0.16	330	
14		Aramid	0.16	330	
15		Glass	0.16	330	
16		Carbon	0.32	330	
17		Aramid	0.32	330	
18		Glass	0.32	330	

The timber sample was hardwood with 15 cm wide, 6 cm deep, and 30 cm long, according to Fig. 1. The bond length of FRP to wood was 15 cm, and the free surface to the end of the wood was 2 cm. The configuration of the timber-FRP system is illustrated in Fig. 2. The specimens are provided with the wet-layup process. Unidirectional fibers of carbon, aramid, and glass with single and double layers (nominal thickness of 0.16 mm) were utilized for specimens. Three popular adhesives were used to stick the FRPs to the timber blocks. The adhesives are epoxy-based from Sika type 30, 300, and 330. The thickness of the adhesive is constant and equal to 0.5 mm approximately. However, it was challenging to provide the exact value of the adhesive thickness due to the wet-layup process.

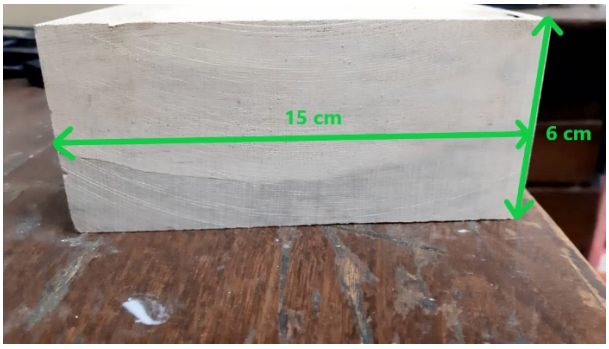

Fig. 1. Details of timber.

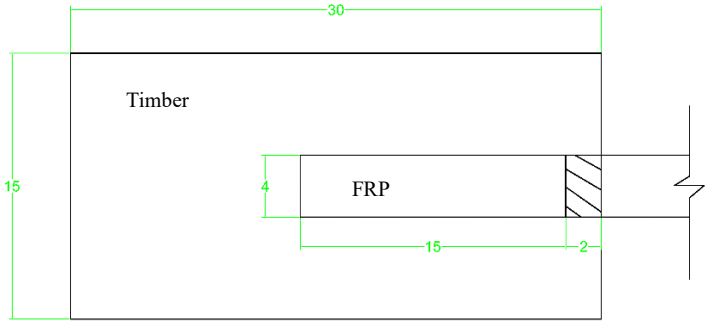

Fig. 2. Configuration of the specimen.

The surface of the timber was cleaned before the composite production by compressed air and acetone. The tests were performed after ten days of manufacturing the composite. They were stored at room temperature of 25 degrees Celsius with 60% humidity. Fig. 3 expresses the test setup, which is a universal testing machine. A slow rate of 0.15 mm/min was used for loading the specimen.

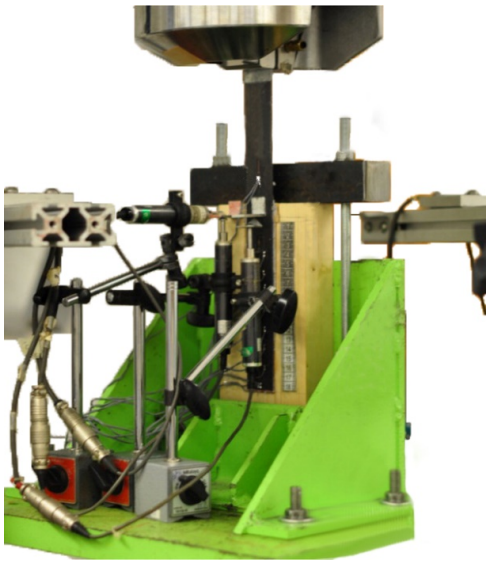

Fig. 3. Universal test setup.

3.2. Material properties

The elasticity modulus and compressive strength of timber were determined by a universal testing machine according to BS 408:2003 (2006). A total of 10 timber samples were tested in parallel and perpendicular directions of the grain. The results of timber properties are shown in Table 3.

Table 3. Timber properties of the experiments.

Material	Grain direction	Elasticity modulus (GPa)	Compressive Strength (MPa)
Timber	Parallel	7.19 (1.4)	34.98 (2.2)
	Perpendicular	0.21 (0.05)	2.9 (0.3)

Note: The parentheses are standard deviations.

To determine the tensile properties of different types of FRPs, tensile test was conducted [54]. Six FRP samples with dimensions of 25 cm and 2.5 cm were prepared by the wet-layup technique. The resulting mechanical properties of all FRP types are expressed in Tables 4.

Table 4. FRP properties of the experiments.

FRP	Fiber	Aerial weight (g/m2)	Tensile Strength (MPa)	Elasticity modulus (GPa)
AFRP	Aramid	380	686 (12%)	65.1 (5%)
CFRP	Carbon	250	591 (9%)	62.3 (7%)
GFRP	Glass	360	513 (11%)	60.0 (7%)

Note: The parentheses are coefficient of variation.

The adhesive mechanical properties were tested according to BS EN ISO 527:1996 [55]. Five samples were prepared according to the standard for each adhesive type. The results are presented in Table 5.

Table 5. Adhesive properties of the experiments.

Adhesive	Elasticity modulus (GPa)	Tensile Strength (MPa)
30	9.22 (0.18)	29.5 (1.5)
300	3.62 (0.05)	51.6 (4.2)
330	4.51 (0.19)	33.3 (1.9)

Note: The parentheses are standard deviations.

3.3. Experimental Results

The ultimate load of each specimen was derived after the test. The values are shown in Table 6. In this table three tests were performed on each sample and the average value was then calculated.

Table 6. Experimental results.

Sample number	Ultimate load (N)				Standard deviation
	Test 1	Test 2	Test 3	Average	
1	22660	22350	23050	22687	350.8
2	18250	17990	18330	18190	177.8
3	15220	16030	14950	15400	562.0
4	33280	32980	33520	33260	270.6
5	30520	29850	30600	30323	411.9
6	27250	27460	27020	27243	220.1
7	20550	20880	19880	20437	509.5
8	17230	16560	19520	17770	1552.1
9	14330	13120	14980	14143	943.9
10	31550	30100	33250	31633	1576.7
11	28660	34360	27670	30230	3610.8
12	18880	18050	19250	18727	614.5
13	19990	20220	25310	21840	3007.3
14	16630	14950	17770	16450	1418.6
15	13860	12660	15660	13927	1701.0
16	29720	30320	28540	29527	905.6
17	26660	28880	24250	26597	2315.6
18	18200	19620	15330	17717	2185.5

According to the experiments, the dominant failure mode was debonding of the timber-FRP interface. Before debonding, the load-slip relation was linear. The crack formation started at the end of the joint and propagated to the unloaded end of the interface. Among adhesive types, type 30 demonstrated higher strength. Adhesive types 300 and 330 showed approximately similar strength; however, type 300 resulted in slightly better strength. Among FRP types, AFRP provided more strength than CFRP, and CFRP illustrated better strength performance than the GFRP. CFRP had approximately 13.3% more strength than GFRP, and almost the similar relation observed between AFRP and CFRP. It should be noted that AFRPs are more expensive than the two others and utilizing them in a project should be based on a reasonable logic.

4. Bayesian Regression Model

The Bayesian linear regression analysis was performed to study the relationship between the output and input variables. Generally, the following equation describes the relationship between the dependent and independent variables:

$$Y = \theta_1 f_1(x) + \theta_2 f_2(x) + \cdots + \theta_d f_d(x) + \varepsilon, \quad (1)$$

where Y is the target or dependent variable, d is the number of input parameters, θ_d is the dth calculated regression coefficient, and $f_d(x)$ is the dth independent variable. ε is the model error. The selection of independent variables is according to the mechanics of the problem and other experiments from the literature. The results are refined by trial and error of considering different possible cases.

In Bayesian linear regression, prior and posterior probabilities are used to update the model parameters. In this algorithm, the error of the model (ε) has a normal distribution with the mean value of zero and the variance of σ^2. Also, the model parameters have the T-distribution, which makes the model capable of evaluating the uncertainty of the model parameters. A prominent privilege of Bayesian regression is that the probability distribution of model parameters and the model error is updated by adding new observations.

Based on experiments performed in this study, and by combining this data with previous experiments of other researchers [8,37]. A comprehensive dataset of 138 experiments was collected. This dataset was employed to train a probabilistic model based on the Bayesian regression analysis. For the regression analysis, 70% of data was randomly separated, and the training proceeded with this data. However, the 30% remaining of the dataset was employed for validation after determining the final model.

As previously mentioned, determining an accurate model is a trial-and-error process. In this regard, different model forms must be defined at the beginning of the analysis. After evaluating the model's accuracy with statistical indices, the next model form is proposed, and the same process is applied. In the process of training the model, several model forms with different variables were tested according to the author's knowledge of effective parameters in bond strength. During the training, applying the Buckingham π theorem to create unitless variables and make the model independent of variables dimensions was tried. After examining these models and omitting the correlated variables due to the same uncertainty source, and merging different effective parameters as a unique variable, the following model was extracted as the best predictive model. According to this equation, an intercept besides three random variables including $\frac{E_{ad}}{E_f}$ as X1, $\frac{A_{ad}}{A_f}$ as X2, and $\frac{S_{ad}}{S_f}$ as X3 are considered.

$$P_u = E_t.A_t[\frac{E_{ad}}{E_f}\theta_1 + \frac{A_{ad}}{A_f}\theta_2 + \frac{S_{ad}}{S_f}\theta_3 + \theta_4 + \varepsilon] \quad (2)$$

where P_u is the ultimate failure load of the system, E_t, E_{ad}, and E_f are the elasticity modulus of timber, adhesive, and FRP, respectively. A_t, A_{ad}, and A_f represent the area of timber, adhesive, and FRP. S_{ad} and S_f are the tensile stress of adhesive and FRP. The coefficients of θ_1 to θ_4 are the outputs of regression analysis, each of which contains a mean value, a standard deviation with a normal distribution, which will be discussed in detail. ε is the model error, where in the Bayesian model has a mean value of zero and a standard deviation value of σ. The standard deviation of the model error has a normal distribution since there is uncertainty in this value (other data lead to a different value). The mean values of θ_1 to θ_4 and the model error values are displayed in Table 7.

Table 7. The output of the Bayesian regression model.

θ_1	θ_2	θ_3	θ_4	σ	R-factor	COV_1	COV_2	COV_3	COV_4
-0.0014147	-8.98836e-7	-0.0119221	0.00110511	8.0108e-5	0.92	15.091	6.349	18.870	4.764

Note: COV is the coefficient of variation in %.

According to this table, the COV of all random variables was less than 0.2 percent, which was an acceptable value. The R-factor was 0.92, demonstrating that the R-squared was 0.85. This value is considered an acceptable prediction value since it is more than 0.7. The correlation matrix of the variables is as follows:

$$\begin{bmatrix} 1 & 0.362 & -0.056 & -0.887 \\ 0.362 & 1 & -0.259 & -0.517 \\ -0.056 & -0.259 & 1 & -0.274 \\ -0.887 & -0.517 & -0.274 & 1 \end{bmatrix}. \quad (3)$$

The correlation of the three random variables is less than 0.5, demonstrating that the variables are independent enough to be unique random variables. It is worth noting that models with almost the same accuracy were derived during the trial and error procedure. However, the random variables in the model forms were highly correlated and were not appropriate to be the best model form. Fig. 4 and 5 illustrate the model prediction versus the observations for training and validation data, respectively. The R-squared for validation data is 0.88. Comparing this value with the training R-squared (0.85), no over-fitting was observed in the training process. According to these figures, training and validation data are well distributed around the bisector line.

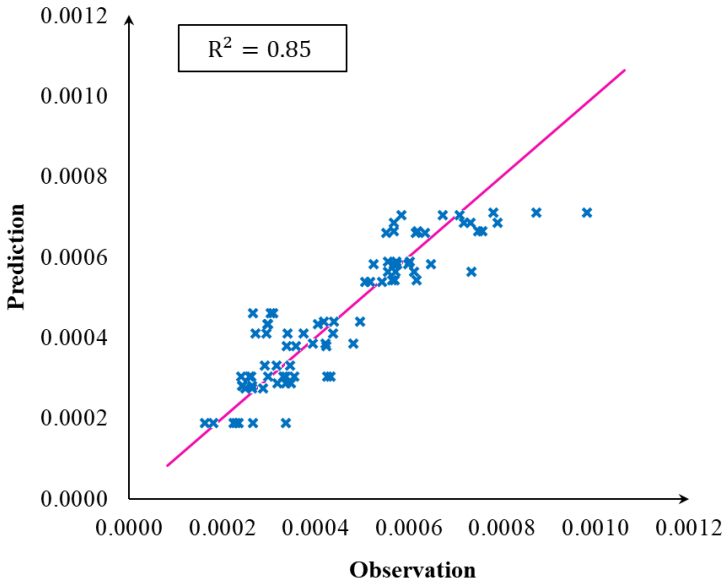

Fig. 4. The observation-prediction diagram of the target value for training data.

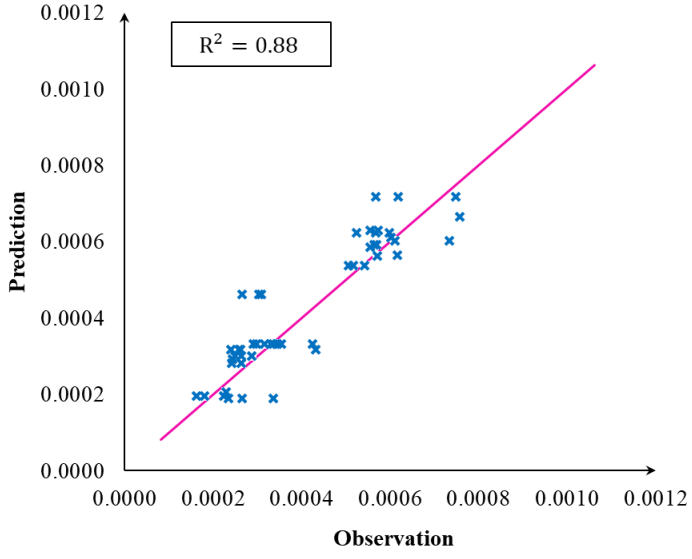

Fig. 5. The observation-prediction diagram of the target value for validation data.

Fig. 6 reveals the residual plots of random variables. Since the variance of residuals was equal over the range of measured values, no heteroskedasticity was observed from this figure. Hence, the analysis results were valid.

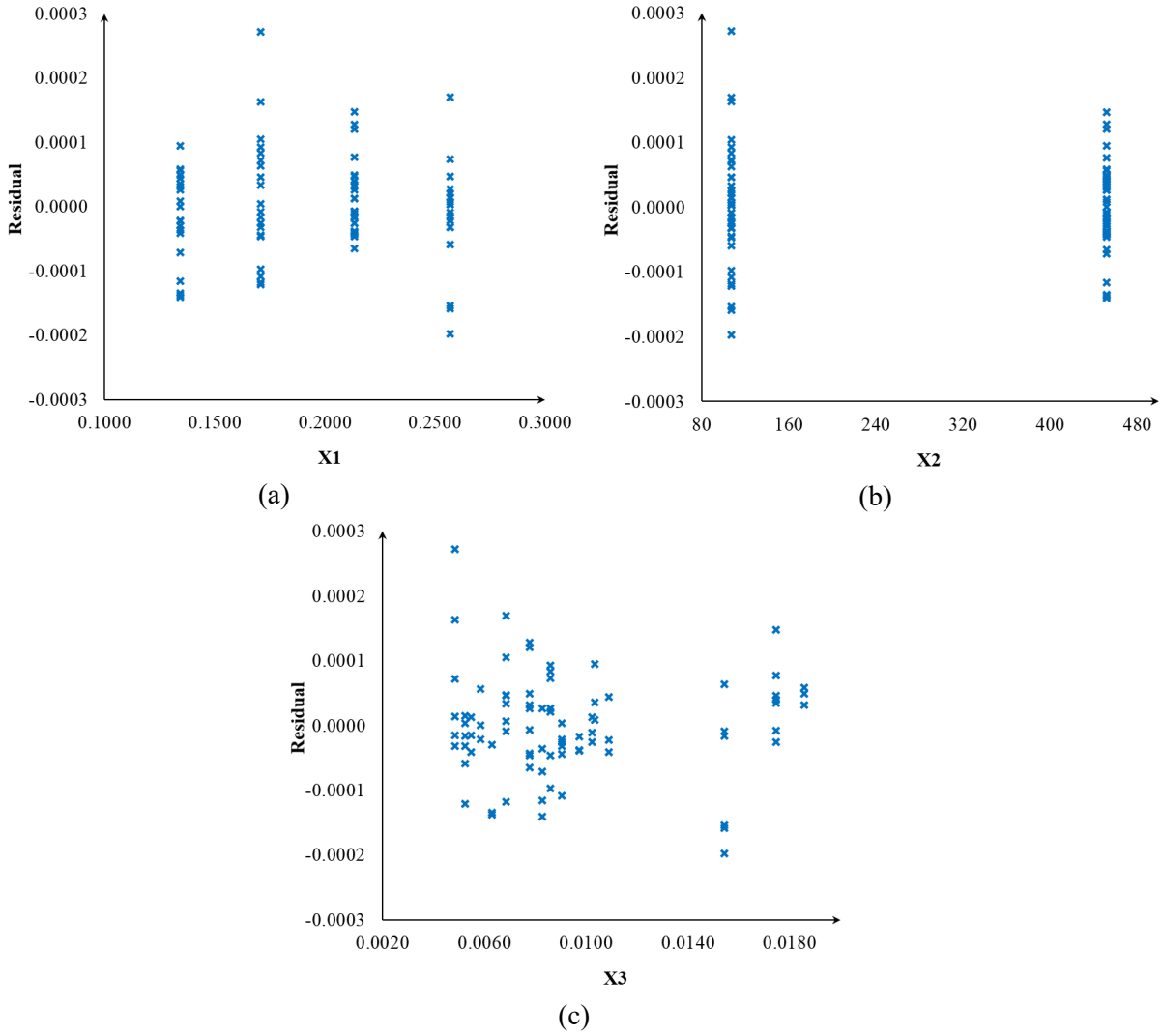

Fig. 6. Residual plot of three random variables, a) x1, b) x2, and c) x3.

5. Reliability Analysis

Since all calculation methods include simplifications, uncertainty always exists in the model. To define the model factor, the following equation can always be defined [56]:

$$P_u^m = \varepsilon \times P_u^c, \quad (4)$$

where P_u^m is the bond strength measure from experiments. P_u^c is the bond strength calculated by the predictive models. ε is the model factor corresponding to any specific model. When the model coefficient is greater than one, it indicates that the calculated resistance is smaller than the measured value and vice versa; The closer the average of this coefficient is to one, the more accurate the model will be. However, coefficients greater than one indicate that the presented model is conservative, and a value less than one implies an unsafe condition.

The model coefficient was calculated for all data presented in the previous sections and for all five introduced models. The average of ε was determined between 0.58 (Palizi and Toufigh model) and 2.94 (Benedetti & Colla model). Based on the average results, Palizi and Toufigh's model was greater than the measured resistance. In contrast, the prediction of the Benedetti and Kola model is much smaller than the measured values. Likewise, in the probabilistic model extracted from the previous

section, this parameter was calculated, and the value of 0.74 was specified, demonstrating the model's acceptable accuracy.

In the reliability analysis, the limit state function for design problems is stated as follows:

$$G = R - D - L, \quad (5)$$

where G is the limit state function, R is the capacity, and D and L are the demand due to dead and live loads, respectively. The resistance function R is generally the capacity of the structural members, such as the moment capacity of a beam. In this research, the resistance function is expressed as the experimental results P_u^m.

$$S_d = \psi \times P_u^c, \quad 6)$$

where S_d is the design load and ψ is the reduction factor for determining an appropriate level of reliability index. When the model factor is not available, the reduction factor can be assumed to be between 0.2 to 0.8.

In this research, to achieve the reliability index of β=3 and based on the calculated coefficient in all six models, the reduction factor was considered approximately equal to 0.6 by trial and error. Considering that timber-FRP strengthening can be performed according to different loading scenarios, three loading levels of 0.75, 1, and 1.25 have been selected based on the live to dead load ratio (η).

By referring to the literature, it was observed that normal, lognormal, and Weibull distributions were the most used for the modulus of elasticity of adhesive and FRP and their yield stress. For the present study, the lognormal distribution was employed due to its popularity and the small standard deviation of the variables. In total, six parameters, including modulus of elasticity, thickness, length, and width of FRP, along with the width and compressive strength of the timber, were considered as the design space, which resulted in a sample space of the size 64 (2^6). Due to three loading levels, the number of reliability analyses was 192 (64 × 3). For each case, the first-order reliability analysis (FORM) method was used to determine the reliability index with the aid of the Hausfer-Lind (1974) method in order to reduce computational cost. The reliability index can be defined geometrically and by finding the distance between the points defined by the expected values of the variables and the closest point on the failure criterion, which can be expressed as follows:

$$\beta = \min\sqrt{(x-\mu)^T C^{-1}(x-\mu)}, \quad (7)$$

where x is the vector of variables with no uncertainties in the limit state function. μ is the mean vector and C is the covariance matrix of the variables with uncertainties.

Overall, two groups of reliability indices were calculated. The first one was related to six models (five models in Table 1 and one probabilistic model proposed in this study) without applying the model coefficient. The second one was with the existence of the model coefficient. When the load ratio is one, the reliability indices based on all six introduced models are determined according to Tables 8 and 9. When the model's uncertainty was not considered in the analysis, the calculated reliability showed the highest value among the two cases. The average reliability index was 4.26 in this case. However, the determined results of the reliability index for all six models were significantly different from each other. The highest average beta was related to model number 5, with an average value of 6.52. This deterministic model was proposed using the genetic programming concept. Also, model number six, the probabilistic model proposed in this research, ranked second with an average reliability index of 6.24. By paying curious attention to the data of tables, the dispersion of the data for each analysis was not very high, and they were in a specific range in this Bayesian model. Whereas, in models 1 to 4, the difference between the results of each analysis was considerable.

As expected, applying uncertainty to the models decreased the reliability index, and its average for all six models approached 2.82. Hence, it can be conceived that neglecting uncertainties in a design process can lead to very inappropriate results. Based on the results acquired, the effect of uncertainty in only six main variables in this research was very significant.

Table 8. Reliability index in 64 cases without considering the model coefficient.

Analysis No.	model 1	model 2	model 3	model 4	model 5	model 6
1	2.11	4.19	5.90	4.32	5.76	5.64
2	3.56	3.59	5.85	4.58	5.55	5.49
3	2.32	5.06	5.83	4.44	5.62	5.76
4	2.46	3.26	5.75	4.96	5.79	5.92
5	2.95	3.11	5.11	4.76	6.26	6.11
6	3.33	3.88	5.18	4.89	6.35	6.18
7	3.70	4.78	5.22	4.55	6.46	6.21
8	2.19	4.11	5.39	4.61	6.42	6.17
9	2.81	4.06	4.44	4.77	6.78	6.15
10	2.43	3.55	4.96	4.36	6.59	6.35
11	2.39	3.18	5.02	4.39	5.96	6.32
12	1.95	3.26	4.40	4.44	5.90	6.38
13	1.86	4.05	4.31	4.29	6.06	6.41
14	1.92	4.09	5.3	5.05	6.01	6.5
15	2.63	4.11	5.23	5.11	6.09	6.46
16	2.81	3.96	5.13	5.21	7.11	6.49
17	3.35	3.62	5.17	5.25	7.18	6.56
18	3.44	3.35	5.33	5.15	7.25	6.49
19	3.02	3.45	4.51	5.18	7.34	6.76
20	2.50	3.40	4.60	4.96	7.27	6.91
21	2.11	3.63	4.73	4.92	7.50	6.85
22	2.62	4.22	4.77	4.98	7.62	6.81
23	3.18	3.55	5.8	4.88	7.66	6.97
24	1.73	3.64	5.85	4.39	7.6	7.01
25	3.13	3.78	5.91	4.75	7.58	7.32
26	4.42	3.11	5.99	4.99	7.71	8.09
27	4.53	3.26	4.84	5.10	7.95	7.96
28	4.60	2.98	4.88	5.14	7.93	7.92
29	4.21	4.16	4.95	5.02	8.05	7.62
30	2.09	4.04	4.96	5.06	8.08	8.56
31	1.96	4.32	5.39	4.55	8.11	8.52
32	1.88	4.38	5.46	4.67	8.01	7.90
33	1.91	4.45	5.55	4.78	7.54	6.13
34	3.40	4.50	5.64	4.82	7.52	6.01
35	1.87	4.64	5.11	4.92	7.59	5.92
36	2.80	4.68	5.16	4.36	7.56	5.69
37	2.76	4.70	5.22	4.21	7.63	5.36
38	2.77	4.22	5.00	4.25	6.32	5.34
39	2.85	4.32	5.03	4.28	6.58	5.2

Continuation of Table 8

40	2.88	4.78	5.11	4.33	6.46	5.29
41	2.11	4.96	5.16	4.16	6.49	5.21
42	2.19	5.15	4.44	4.46	6.59	5.18
43	2.34	5.19	4.49	4.49	6.41	5.46
44	2.39	5.17	4.55	4.28	6.11	5.39
45	2.08	5.23	4.59	4.35	5.95	5.84
46	1.28	5.14	5.41	4.74	6.06	5.52
47	2.31	4.80	5.46	4.84	5.90	5.66
48	3.45	4.76	5.52	4.89	5.78	5.11
49	3.18	4.44	5.59	4.82	5.86	5.19
50	4.04	4.39	5.79	4.94	5.32	6.23
51	2.23	4.67	5.84	4.99	5.36	6.36
52	2.44	4.75	5.89	4.59	5.39	6.6
53	2.96	4.82	5.92	4.65	5.44	6.52
54	2.33	4.64	4.5	4.71	5.26	6.46
55	2.19	4.40	4.56	4.88	5.29	5.95
56	3.18	4.16	4.61	4.31	6.11	5.91
57	3.25	3.76	4.67	4.35	6.26	5.9
58	2.61	3.57	4.73	4.36	6.31	5.85
59	2.64	3.22	4.78	4.44	6.35	5.75
60	1.36	3.56	4.82	4.41	5.25	5.73
61	1.96	3.49	4.36	4.72	5.18	5.45
62	1.85	3.32	4.42	4.62	5.15	5.49
63	2.22	3.71	4.44	4.63	5.21	5.51
64	3.16	3.19	4.55	4.69	5.25	5.19
Mean	2.67	4.09	5.11	4.70	6.52	6.24
Total Mean	4.26					

Table 9. Reliability index in 64 cases considering the model coefficient.

Analysis No.	model 1	model 2	model 3	model 4	model 5	model 6
1	1.29	2.51	3.15	2.18	3.20	3.08
2	2.16	2.11	3.11	2.25	3.10	3.00
3	1.39	3.03	3.05	2.11	3.14	3.15
4	1.48	1.95	3.01	2.21	3.19	3.23
5	1.79	1.82	2.75	2.43	3.50	3.34
6	2.04	2.32	2.80	2.49	3.55	3.38
7	2.27	2.86	2.82	2.32	3.61	3.39
8	1.34	2.41	2.88	2.35	3.50	3.43
9	1.70	2.43	2.33	2.43	3.79	3.42
10	1.49	2.13	2.61	2.11	3.68	3.53
11	1.46	1.86	2.71	2.24	3.33	3.51
12	1.20	1.95	2.33	2.27	3.18	3.54
13	1.14	2.43	2.30	2.19	3.39	3.56
14	1.18	2.41	2.82	2.50	3.36	3.61

Continuation of Table 9

15	1.60	2.46	2.83	2.61	3.45	3.59
16	1.72	2.37	2.77	2.66	3.93	3.65
17	2.06	2.14	2.79	2.68	3.97	3.69
18	2.08	2.01	2.80	2.57	4.01	3.65
19	1.85	2.07	2.44	2.64	4.06	3.80
20	1.51	1.97	2.49	2.53	4.02	3.88
21	1.27	2.17	2.50	2.43	4.14	3.85
22	1.61	2.41	2.58	2.54	4.21	3.83
23	1.95	2.13	3.14	2.49	4.23	3.92
24	1.06	2.18	3.04	2.24	4.20	3.89
25	1.90	2.16	3.19	2.30	4.19	4.07
26	2.71	1.86	3.24	2.55	4.26	4.49
27	2.78	1.91	2.56	2.60	4.39	4.42
28	2.82	1.66	2.64	2.62	4.38	4.40
29	2.58	2.49	2.68	2.56	4.45	4.23
30	1.28	2.42	2.68	2.58	4.46	4.76
31	1.20	2.59	2.91	2.32	4.48	4.84
32	1.15	2.62	2.86	2.38	4.43	4.49
33	1.17	2.61	3.00	2.35	4.17	3.48
34	2.04	2.69	3.05	2.46	4.15	3.41
35	1.11	2.56	2.70	2.51	4.19	3.36
36	1.72	2.49	2.79	2.22	4.18	3.23
37	1.69	2.81	2.82	2.05	4.22	3.05
38	1.70	2.53	2.61	2.17	3.57	3.00
39	1.75	2.59	2.66	2.18	3.72	2.92
40	1.65	2.86	2.76	2.21	3.65	3.01
41	1.29	2.90	2.79	2.04	3.67	2.96
42	1.34	3.01	2.40	2.28	3.72	2.94
43	1.40	3.11	2.43	2.29	3.62	3.10
44	1.47	3.10	2.35	2.01	3.45	3.06
45	1.28	3.08	2.48	2.22	3.27	3.32
46	0.79	3.08	2.92	2.42	3.33	3.14
47	1.42	2.87	2.95	2.48	3.24	3.22
48	2.09	2.85	2.85	2.49	3.18	2.90
49	1.95	2.61	3.02	2.55	3.22	2.95
50	2.48	2.58	3.02	2.52	2.92	3.54
51	1.37	2.80	3.16	2.51	2.95	3.61
52	1.50	2.84	3.18	2.34	2.96	3.75
53	1.82	2.89	3.20	2.37	2.99	3.70
54	1.40	2.71	2.35	2.40	2.89	3.57
55	1.34	2.63	2.46	2.49	2.91	3.29
56	1.95	2.49	2.49	2.11	3.36	3.27
57	1.92	2.25	2.52	2.22	3.44	3.26
58	1.60	2.08	2.48	2.14	3.47	3.23
59	1.62	1.93	2.58	2.27	3.49	3.18

Continuation of Table 9

60	0.80	2.10	2.61	2.25	2.88	3.17
61	1.20	2.09	2.36	2.41	2.85	3.01
62	1.13	1.96	2.25	2.36	2.83	3.03
63	1.36	2.18	2.40	2.36	2.86	3.04
64	1.94	1.88	2.46	2.32	2.88	2.87
Mean	1.63	2.42	2.73	2.37	3.61	3.49
Total Mean	2.82					

In Fig. 7, the reliability index from the FORM analysis is plotted in terms of the ratio of the live to dead load defined earlier. As mentioned, three load ratios of 0.75, 1, and 1.25 were considered. According to this figure, the level of the reliability index becomes much more uniform considering the model coefficient and regardless of the model type. The reduction of the beta reliability index for the case without considering the model coefficient was quite clear when the load ratio increased, and a particular decreasing trend could be seen in its diagram. On the other hand, no particular trend was captured considering the uncertainties, and the variation range of the index exhibited a uniform value regardless of the model type. This result is consistent with the other study [57].

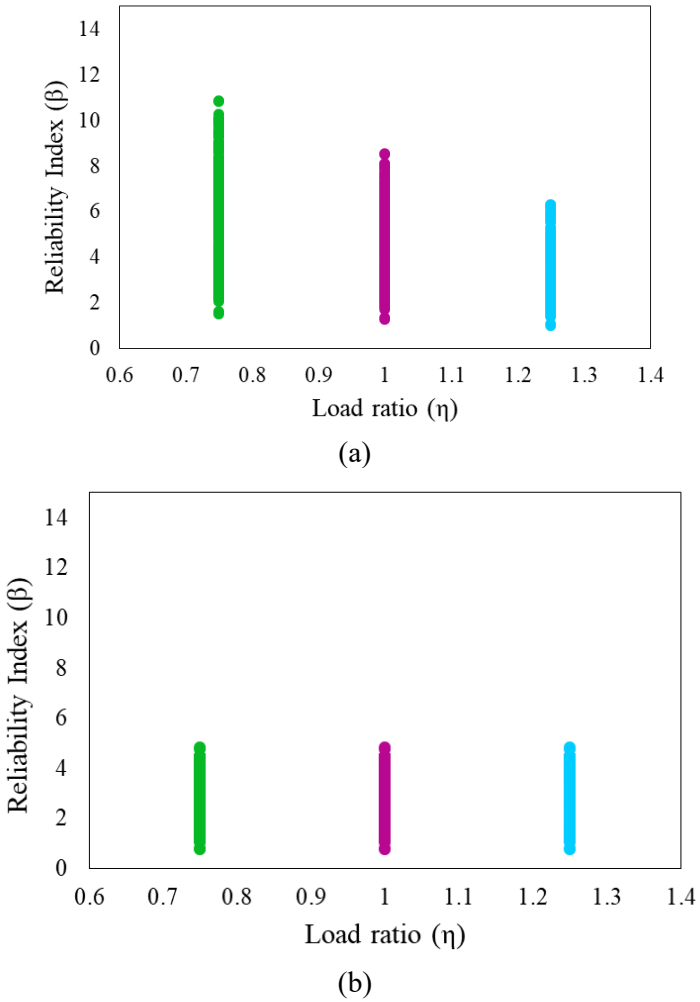

Fig. 7. The reliability index versus variation of load ratio, a) without considering the uncertainty, b) with uncertainties.

Table 10.

Design variant	Road pavement structure	Symbols
1	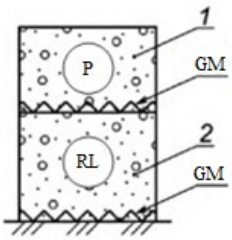	1 – binder-treated pavement layer 2 – reinforced base layer GM – geosynthetic material
2	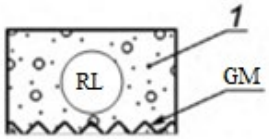	1 – reinforced base layer GM – geosynthetic material
3	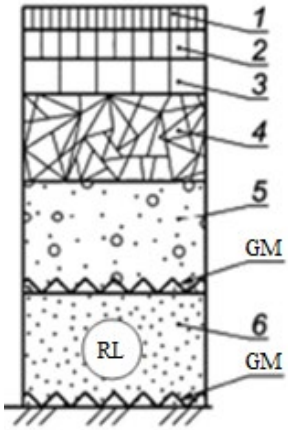	1, 2 – covering layers 3, 4, 5 – base layers 6 – reinforced additional base layer GM – geosynthetic material

4. CONCLUSIONS

In this research, a probabilistic approach was employed to assess the models in the design process of timber-FRP composites. First, an experimental program was implemented to investigate the bond strength of the timber-FRP system. Afterward, the data of the experiments was combined with other data from the literature, and a comprehensive set was collected. The dataset was then applied to Bayesian regression analysis, and a probabilistic formulation was derived. Besides the new proposed model, few existing deterministic models were collected from the literature to investigate all models' reliabilities. The reliability index of all models was calculated under three different load ratios of 0.75, 1, and 1.25. The following highlights were achieved in this study:

- According to the experimental study, AFRP had the best strength performance in timber-FRP composites. However, GFRP was the weakest among all three tested FRPs (AFRP, CFRP, and GFRP).
- The experiments demonstrated that using hardwood instead of softwood caused the failure mode of the timber-FRP pull-out test to be debonding of adhesive and FRP.
- Although three types of adhesives with approximately similar properties were employed in this study, the adhesive type also affected the bond strength value.
- The probabilistic-based models seemed more reliable since uncertainties have been considered in the formulation process.
- Considering the uncertainties in deterministic models, the reliability index decreased notably. It should be noted that the uncertainty of only six variables was considered in this research.

- Increasing the load ratio in the limit state function decreased the reliability index when uncertainties were not considered.
- As expected, the load ratio effect in the reliability index was removed when the uncertainties were considered.

These findings underscore the significance of accounting for uncertainties in the design and analysis of timber-FRP composites. The probabilistic approach offers a more robust and reliable framework, enhancing the understanding of the performance and reliability of these composites. By considering uncertainties, engineers and practitioners can make informed decisions and develop more accurate design guidelines for timber-FRP systems, ultimately ensuring their structural integrity and performance in real-world applications.

REFERENCES

1. Babatunde S.A. Review of strengthening techniques for masonry using fiber reinforced polymers. Compos Struct. 2017. 161. P. 246 – 255. https://doi.org/10.1016/j.compstruct.2016.10.132
2. Carney P., Myers J.J. Shear and flexural strengthening of masonry infill walls with FRP for extreme out-of-plane loading. Archit Eng Build Integr Solut. 2003. 40699 P. 246 – 250. https://doi.org/10.1061/40699(2003)45
3. Yavartanoo F., Kim C.S., Bolhassani D., Kang T.H.K. Macro-modeling of CFRP strengthening in U-shaped masonry walls under combined vertical and out-of-plane loads. Eng Fail Anal. 2025. 177. 109664. https://doi.org/10.1016/j.engfailanal.2025.109664
4. Yip C.L., Sugiman S., Chin D., Ahmad H. Experimental and numerical investigation of adhesively bonded kfrp/steel double strap joints incorporating eggshell powder-toughened epoxy adhesive. Case Stud Constr Mater. 2024. 20. e02790. https://doi.org/10.1016/j.cscm.2023.e02790
5. Abdulwahed L.R. A novel probabilistic approach to the plastic analysis of steel moment frames. Asian J Civ Eng. 2023. 24. P. 1001 – 1014.
6. Idan M.H., Hussain R.G.K., Mohammed M.A. Preparation and Study of the Effect of Cobalt and Magnesium on the Structural and Optical Properties of Cadmium Sulfide Compound. J Nanostructures. 2022. 12. P. 921 – 931. https://doi.org/10.22052/JNS.2022.04.0149.
7. Liu W., Tan S. Carbon nanotubes (CNTs) and short-aramid-fiber epoxy (SAFE) toughened adhesive joints between bamboo scrimber and steel substrates treated with resin pre-coating (RPC) method. Int J Adhes Adhes. 2025. 140. 104011. https://doi.org/10.1016/j.ijadhadh.2025.104011
8. Yin Y., Cheng H. The influence of multiple CFRP reinforcement forms on the interface bonding performance of timber beam-column joint areas. J Phys Conf Ser. 2025. 3006. https://doi.org/10.1088/1742-6596/3006/1/012024
9. Mohammed A.R., Abdulwahed L.R., Rashid B. Seismic structural analysis of multi-story concrete building based on halabja 2017 earthquake. J Eng Sci Technol. 2022. 27. P. 4092 – 4206.
10. Muaamar Hasan Idan, Raheem G. Kadhim MAM. Preparation and study of the effect of adding cobalt and magnesium on the morphological, optical properties and bacterial activity of cadmium sulfide compound. 2023. 2977. 040117.
11. Raftery G.M., Karami Z., Pizzi A., Nicholson C.L. Durability assessment of one-component polyurethane adhesives for bonding of preservative treated wood subject to artificial ageing. Int J Adhes Adhes. 2024. 129. 103594. https://doi.org/10.1016/j.ijadhadh.2023.103594
12. Khateeb A.H., Abdulwahed L.R., Mohammed A.R. Modeling vibration and crack behavior of reinforced concrete beams : developing artificial neural network predictive models. Asian J Civ Eng 2023. https://doi.org/10.1007/s42107-023-00763-6
13. O'Ceallaigh C., McGetrick P.J., Walsh T., Moran G., Sikora K., Mcpolin D. et al. Creep behaviour and creep recovery of FRP reinforced timber elements. Wood Mater Sci Eng 2025. 0272. P. 1 – 9. https://doi.org/10.1080/17480272.2025.2480248

14. Aymen R. Mohammed, Larah R. Abdulwahed OAQ. Structural comparison study on composite steel girder bridges between iraqi and AASHTO bridge live loads. AIP Conf. Proc., 2024.
15. Patil V.S., Patil A.Y., Kumar P., Kumar A., Kumar R., Prakash C. et al. Enhancing material properties with a sustainable wood-quartz-HDPE composite: a study on strength. Cogent Eng. 2025. 12. https://doi.org/10.1080/23311916.2024.2434946
16. Hitka M., Naď M., Klement I., Sydor M. Improving joint strength through controlled wood swelling. Wood Mater Sci Eng. 2025. 0272. P. 1 – 10. https://doi.org/10.1080/17480272.2025.2466844
17. Kawecki B. Numerical Modelling and Experimental Testing on Polyurethane Adhesively Bonded Joints Behaviour in Wood-Wood and Wood-Carbon Fibre Reinforced Polymer Layouts. Adv Sci Technol Res J. 2023. 17. P. 36 – 52. https://doi.org/10.12913/22998624/159723
18. Mohammed M.A. CoS THIN FILM DEPOSITED BY CHEMICAL SPRAY ENGINEERING TECHNIQUE: OPTICAL, GAS-SENSING AND STRUCTURAL CHARACTERISTICS. Procedia Environ Sci Eng Manag. 2024. 11. P. 433 – 440.
19. Mukhtar F., Jawdhari A. RC beams flexurally strengthened with CFRP sheets combined with FRC layer for mitigating debonding failures. Constr Build Mater. 2024. 427. 136274. https://doi.org/10.1016/j.conbuildmat.2024.136274
20. Mohammed M.A. The Effect of Substrate Temperature on the Nanostructured V2O5 Thin Films, Studying Their Structural, Optical Properties and Testing as Gas Sensors. J Nanostructures. 2025. 15. P. 200 – 209. https://doi.org/10.22052/JNS.2025.01.019
21. Kopraman Y., Özdemir A., Anıl Ö., Sakin S., Armakan F. Experimental investigation of bond–slip behavior of between-anchored steel strips to concrete surface. Arch Civ Mech Eng. 2022. 22. P. 1 – 19. https://doi.org/10.1007/s43452-022-00523-4
22. Alshaeer F., Mohammed M.A., Zorah M., Alharbi N., Mahmoud H.A.M.A., Ahmed A.M.E., et al. Synergistic defect passivation and charge transport enhancement via thiosemicarbazide-functionalized carbon nanotubes for high-efficiency lead-free $CsSnI_3$ perovskite solar cells: A pathway to 23.34 % efficiency. J Alloys Compd. 2025. 1026. P. 180428. https://doi.org/10.1016/j.jallcom.2025.180428
23. Kodur V.K.R., Naser M.Z., Kim H.S. Fire performance of concrete structures incorporating FRP reinforcement : State-of-the-art and knowledge gaps. Cem Concr Compos 2025. P. 161.
24. Jassim N.M., Ibrahim N.I., Khalaf N.Z. Z-scan Study of the Non-linear Optical Properties of Silver/Curcumin Dye Nanocomposites Prepared Via Nanosecond Pulsed Laser Ablation. Rev Des Compos Des Mater Av. 2024. 34. P. 533 – 540. https://doi.org/10.18280/rcma.340415
25. Li S., Hadigheh S.A. Enhancing the load-slip behaviour of cross-laminated timber-concrete composite using FRP connections: Experimental and numerical investigation. Eng Struct. 2025. 336. https://doi.org/10.1016/j.engstruct.2025.120479
26. Jassim N.M. Synthesis and nonlinear optical responses of Ag: ZnO core: shell nanoparticles induced by Z-scan technique. J Opt. 2024.6. 02432. https://doi.org/10.1007/s12596-024-02432-6
27. Rebouh R., Benzaamia A., Ghrici M. Bayesian – optimized tree – based models for predicting the shear strength of U – shaped externally bonded FRP – strengthened RC beams. Asian J Civ Eng. 2025. 26. P. 1465 – 1478. https://doi.org/10.1007/s42107-024-01258-8
28. Jassim N.M., Wang K., Han X., Long H., Wang B., Lu P. Plasmon assisted enhanced second-harmonic generation in single hybrid Au/ZnS nanowires. Opt Mater (Amst). 2017. 64. P. 257 – 261. https://doi.org/10.1016/j.optmat.2016.11.034
29. Dizayee W., Hamarashid M.M., Zorah M., Mahmoud H.A.M.A, Al-Bahrani M., Taki A.G. et al. Synergistic effect of Ni(OH)2 and MXene nanosheets in 3D framework on the improvement of dielectric, energy storage, mechanical and thermal characteristics of polyvinylidene fluoride(PVDF) polymeric composites. J Alloys Compd. 2024. 1004. 175825. https://doi.org/10.1016/j.jallcom.2024.175825

30. Kaiser H., Karbhari V.M. Identification of potential defects in the rehabilitation of concrete structures with FRP composites. Int J Mater Prod Technol. 2003. 19. P. 498 – 520.
31. Samawi K.A., Mohammed B.A., Salman E.A.A., Mahmoud H.A.M.A., Sameen A.Z., Mohealdeen S.M. et al. Vertical growth of a 3D Ni-Co-LDH/N-doped graphene aerogel: a cost-effective and high-performance sulfur host for Li-S batteries. Phys Chem Chem Phys. 2024. 26. P. 9284 – 9594. https://doi.org/10.1039/d3cp05716j
32. Atadero R.A., Karbhari V.M. Sources of uncertainty and design values for field-manufactured FRP. Compos Struct. 2009. 89. P. 83 – 93. https://doi.org/10.1016/j.compstruct.2008.07.001
33. Samawi K.A., Salman E.A.A., Hasan H.A., Mahmoud H.A.M.A., Mohealdeen S.M., Abdulkareem-Alsultan G. et al. Single-atom cobalt encapsulated in carbon nanotubes as an effective catalyst for enhancing sulfur conversion in lithium-sulfur batteries. Mol Syst Des Eng. 2024. 9. P. 464 – 476. https://doi.org/10.1039/d3me00191a
34. Stergiou K., Ntakolia C., Varytis P., Koumoulos E., Karlsson P., Moustakidis S. Enhancing property prediction and process optimization in building materials through machine learning: A review. Comput Mater Sci. 2023. 220. 112031. https://doi.org/10.1016/j.commatsci.2023.112031
35. Toufigh V., Palizi S. Performance evaluation of slag-based concrete at elevated temperatures by a novel machine learning approach. Constr Build Mater. 2022. 358. 129357. https://doi.org/10.1016/j.conbuildmat.2022.129357
36. Ben Chaabene W., Flah M., Nehdi M.L. Machine learning prediction of mechanical properties of concrete: Critical review. Constr Build Mater. 2020. 260. 119889. https://doi.org/10.1016/j.conbuildmat.2020.119889
37. Palizi S., Toufigh V. Fire-induced damage assessment of cementless alkali-activated slag-based concrete. Constr Build Mater. 2023. 393. 132002. https://doi.org/10.1016/j.conbuildmat.2023.132002
38. Hassan A., Samawi K.A., Nassar M.F., Haddad R., Roostaie A., Sadeghzadeh S.M. Synthesis of Cyclic Carbonate from Carbon Dioxide and Epoxides Using Bicobalt Complexes Absorbed on DFNS. Catal Letters. 2023. 153. P. 2900 – 2909. https://doi.org/10.1007/s10562-022-04130-z
39. Atadero R.A., Karbhari V.M. Calibration of resistance factors for reliability based design of externally-bonded FRP composites. Compos Part B Eng. 2008. 39. P. 665 – 679. https://doi.org/10.1016/j.compositesb.2007.06.004
40. Alsultan A.G., Asikin-Mijan N., Obeas L.K., Islam A., Mansir N., Teo S.H. et al. Selective Deoxygenation of Sludge Palm Oil into Diesel Range Fuel over Mn-Mo Supported on Activated Carbon Catalyst. Catalysts. 2022. 12. P. 1 – 15. https://doi.org/10.3390/catal12050566
41. Zhou Y., Zhang J., Li W., Hu B., Huang X. Reliability-based design analysis of FRP shear strengthened reinforced concrete beams considering different FRP configurations. Compos Struct. 2020. 237. 111957. https://doi.org/10.1016/j.compstruct.2020.111957
42. Alshaeer F., obeas L kareem, Zorah M., Mahmoud H.A.M.A., Abdalgadir L.M., Taki A.G. et al. Bandgap-engineered MXene-g-C3N4 interfacial layer for enhanced charge carrier dynamics in perovskite solar cells. J Alloys Compd. 2025. 1011. 178247. https://doi.org/10.1016/j.jallcom.2024.178247
43. Ali O., Bigaud D., Riahi H. Seismic performance of reinforced concrete frame structures strengthened with FRP laminates using a reliability-based advanced approach. Compos Part B. 2018. 139. P. 238 – 248. https://doi.org/10.1016/j.compositesb.2017.11.051
44. Yang F., Gan W., Chen B., Wu J., Yuan S. Experimental Study on Bond Fatigue Between Carbon Fiber-Reinforced Polymer Bars and Seawater–Sea Sand Concrete Under Seawater Immersion and Dry–Wet Cycle Conditions. Buildings 2025;15. https://doi.org/10.3390/buildings15030438

45. Chang X., Wang X., He Z., Ding L., Yuan K., Noori M. et al. Damage identification and localization of pultruded FRP composites based on convolutional recurrent neural network and metaheuristic intelligent algorithms. Polym Compos. 2025. https://doi.org/10.1002/pc.29845
46. Alharbi N., Alotaibi M.M., Obeas L.K., Marhoon I.I,. Zorah M., Taki A.G. et al. Boosting efficiency and long-lifespan in perovskite solar cells via 2D-MXene/Janus MoSSe integration. J Alloys Compd. 2025. 1013. 178501. https://doi.org/10.1016/j.jallcom.2025.178501
47. Zhang D., Gu X., Yu Q., Huang H., Wan B. Fully probabilistic analysis of FRP-to-concrete bonded joints considering model uncertainty. Compos Struct. 2018. 185. P. 786 – 806. https://doi.org/10.1016/j.compstruct.2017.11.058
48. Benedetti A., Colla C. Strengthening of old timber beams by means of externally bonded reinforcement. 11th World Conf Timber Eng 2010, WCTE 2010. 2010. 3. P. 2053 – 2058.
49. Juvandes L.F.P., Barbosa R.M.T. Bond analysis of timber structures strengthened with FRP systems. Strain. 2012. 48. P. 124 – 135. https://doi.org/10.1111/j.1475-1305.2011.00804.x
50. Dizayee W., Ahmed M., Zorah M., Mahmoud H.M.A., Shabbir M., Abdulkareem-alsultan G. et al. Lightweight and broadband NiO. Ni. borophene foams for enhanced electromagnetic wave attenuation. J Sci Adv Mater Devices. 2025. 10.100934. https://doi.org/10.1016/j.jsamd.2025.100934
51. Yuldasheva S., Fayzullaev N., Khamdamova S., Fawzi M. Enhanced tetracycline degradation in pharmaceutical wastewater via S-scheme photocatalysis using graphydine quantum dots. Janus MoSSe heterostructures. J Water Process Eng. 2024. 68. 106470. https://doi.org/10.1016/j.jwpe.2024.106470
52. Wan J., Smith S.T., Asce F., Qiao P., Asce F., Chen F. Experimental Investigation on FRP-to-Timber Bonded Interfaces. J Compos Constr. 2014. P. 1 – 9. https://doi.org/10.1061/(ASCE)CC.1943-5614.0000418
53. Vahedian A., Shrestha R., Crews K. Effective bond length and bond behaviour of FRP externally bonded to timber. Constr Build Mater. 2017. 151. P. 742 – 754. https://doi.org/10.1016/j.conbuildmat.2017.06.149
54. Sullivan K., Peterman K.D. A review of adhesive steel-to-steel connections for use in heavy construction. J Constr Steel Res. 2024. 213. 108405. https://doi.org/10.1016/j.jcsr.2023.108405
55. Standard B. Plastics Determination of tensile properties. BS EN ISO. 1996. 28. P. 1. https://doi.org/10.1016/S0091-679X(08)61633-7
56. Phoon K.K., Kulhawy F.H. Characterisation of model uncertainties for laterally loaded rigid drilled shafts. Géotechnique. 2005. P. 45 – 54.
57. Huang Q., Liu Y., Guo Z., Ju J.W.W. Flexural fatigue strength of RC bridge girders strengthened by PHSW-PM. Eng Struct. 2025. 338. 120640. https://doi.org/10.1016/j.engstruct.2025.120640

INFORMATION ABOUT THE AUTHOR

Larah R. Abdulwahed, dr.larah.riyadh@mtu.edu.iq, ORCID ID: https://orcid.org/0000-0003-4404-7700, SCOPUS: https://www.scopus.com/authid/detail.uri?authorId=57204160332, Middle Technical University, Engineering Sciences (Ph.D.), Associate Professor of Civil Engineering